Macromolecules

Article

pubs.acs.org/Macromolecules

High-Efficiency Cell-Penetrating Helical Poly(phenyl isocyanide) Chains Modified Cellular Tracer and Nanovectors with Thiol Ratiometric Fluorescence Imaging Performance

Xin Han, Jian Zhang, Chen-Yang Qiao, Wen-Ming Zhang, Jun Yin,* and Zong-Quan Wu

Department of Polymer Science and Engineering, School of Chemistry and Chemical Engineering, Hefei University of Technology and Anhui Key Laboratory of Advanced Functional Materials and Devices, Hefei 230009, China

Supporting Information

ABSTRACT: In order to precisely tail the endocytosis process and determine the internal location of drug carriers in cells, fluorescent tracers with high sensitivity and versatility are one of the most powerful tools. Nevertheless, conventional single fluorescent probes always suffered from the interference of background fluorescence or the lack of long-time monitoring capability, resulting in the low resolution and efficiency. To overcome this drawback, nanocarriers capable of multicolor fluorogenic and ratiometric properties became an urgently needed solution. In this contribution, starting from pentafluorophenyl ester (PFP)- and tetraphenylethene (TPE)-functionalized phenyl isocyanide (PI) monomers as well as L-hydrophilic (HP) PI monomers, a type of well-defined amphiphilic block copolymer, P(PFPPI-*co*-TPEPI-*co*-HPPI)-*b*-HPPPI, with controlled molecular weights and tunable compositions was prepared through sequential living copolymerization with phenylethynyl Pd(II) complex as a single catalyst in one pot. Disulfide bonds were then introduced by the exchange reaction between PFP units and cystamine (Cys; a degradable cross-linker). The resultant P(CysPI-*co*-TPEPI-*co*-HPPI)-*b*-HPPPI copolymers showed a time-dependent disruption in the conditions mimicking the intracellular reducing environment and an aggregation-caused quenching (ACQ) optical behavior that they were emissive when single chain dispersed but became nonfluorescent if the polymer chains were aggregated. Thanks to such a unique optical phenomenon, nanocarriers capable of fluorescence ratiometric property could be constructed after incorporating another solvatochromic dye, Nile red (NR), in water. This new class of core cross-linked NR@P(CysPI-*co*-TPEPI-*co*-HPPI)-*b*-HPPPI micelles not only exhibited excellent fluorescence ratiometric cell imaging ability but also possessed rapid cell membrane permeability due to the PEGylated single left-handed helical PPI corona and exposed the real-time disintegration of nanocarriers in front of us. Fatal and irreversible damage to cancer cells could be achieved by the high-efficiency delivery of chemotherapeutic agents. We speculate that these newly developed fluorescent integrated nanocarriers can potentially be utilized as a promising approach to cancer diagnosis and therapy.

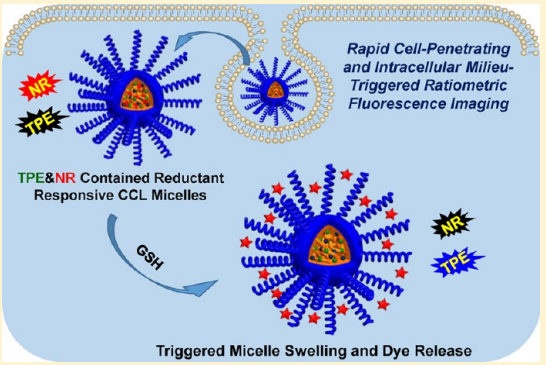

INTRODUCTION

"Imaging guided therapy", with both imaging capability and therapeutic effect, in cancer treatment has attracted increased attention.[1−4] For this purpose, development of high-efficiency cellular tracers and drug nanocarriers is of great scientific importance and has great value in practical application because it enables researchers to systematically monitor the tumor location and size and evaluate the therapeutic effect in real time.

Polymeric micelles are one of the ideal nanocarriers that they can not only enhance the drug solubility, prolong in vivo circulation time, but also increase the cellular uptake efficiency, especially targeted units are functionalized on the micellar surface.[5−14] However, due to the thermodynamic equilibrium, conventional self-assembled micelles may suffer from disintegration when the concentration reaches or below the critical association concentration (CAC), leading to premature release of encapsulated drugs before reaching the target tissues and resulting in reduced therapeutic efficacy.[15,16] To solve this problem, core cross-linked (CCL) micelles have been developed as an effective approach to fix the micellar structure and permanently suppress the dissociation.[17−20] Up to now, several CCL methods were emerged, including ionic interaction,[21−23] condensation reaction,[24,25] photo-cross-linking reaction,[26,27] and "click" reaction,[28] etc. But in the case of drug delivery systems, the polymeric micelles must dissociate or swell to release entrapped drugs at the targeted site. For this purpose, stimuli-responsive degradability endow them ideal candidates for such utilization.[21,22,29−35] Taking redox, for example, the cleavage of the disulfide bond would occur within the cell because of the high intracellular reducing environment with a concentration of ∼3−10 mM glutathione.[36,37]

Received: March 30, 2017
Revised: May 21, 2017
Published: May 30, 2017

DOI: 10.1021/acs.macromol.7b00669
Macromolecules 2017, 50, 4114−4125

Scheme 1. Synthetic Routes Employed for the Successive Copolymerization of Pentafluorophenyl Ester-Functionalized Phenyl Isocyanide Monomers (PFPPI; M_1), Tetraphenylethene (TPE)-Functionalized Phenyl Isocyanide Monomers (TPEPI; M_2), and L-Hydrophilic Phenyl Isocyanide Monomers (HPPI; M_3) by Living Polymerization with Phenylethynyl Pd(II) Complex as a Single Catalyst To Form P(PFPPI-*co*-TPEPI-*co*-HPPI)-*b*-HPPPI Block Copolymers in One Pot

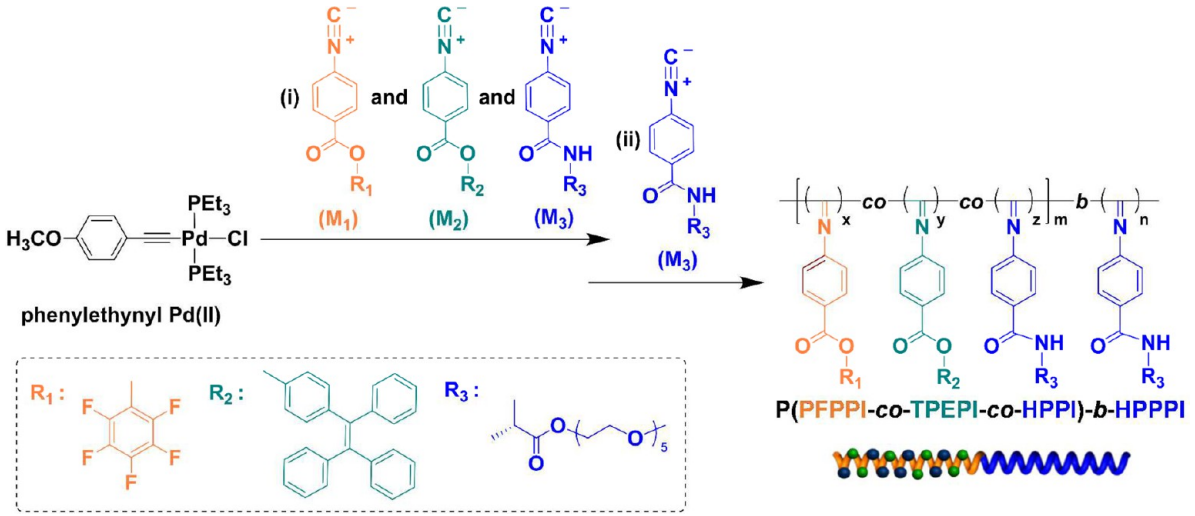

So far, fluorescent molecules are probably the most used biological imaging reagents, and various approaches have been developed in order to increase their accumulation and extend their retention time within cells, such as physical encapsulation by biocompatible polymers or directly in situ covalent attachment to polymer chains.[38−45] Since Tang et al. observed the unique photophysical process termed as "aggregation-induced emission (AIE)",[46,47] a variety of AIE fluorogens, such as tetraphenylsilole (TPS),[48,49] tetraphenylethene (TPE),[50−54] triphenylethene,[55−58] and distyrylanthracene,[59−61] have emerged and opened the door for a new direction for cellular tracers design. For example, Tang et al. reported a new type of fluorescence "turn-on" probe for tracing live cells over a long period of time.[62] In their design, a large number of tetraphenylethene (TPE) molecules were labeled to a chitosan (CS) chain; the resultant TPE-CS bioconjugate was non-fluorescent when dissolved but became highly emissive once aggregated. The cellular staining by the TPE-CS aggregates enabled persistent cell tracing for as long as 15 passages. Furthermore, the internalized AIE aggregates are kept inside the cellular compartments and do not contaminate other cell lines in the coculture systems, permitting the differentiation of specific cancerous cells from normal healthy cells. Similarly, Wei et al. developed fluorescent polymeric nanoparticles with the hydrophobic AIE core covered by a hydrophilic poly(ethylene glycol) or glucose-containing shell.[63−65] Both of them exhibited excellent fluorescence performance and good dispersibility in aqueous solution, allowing them to be used in bioimaging applications. On the contrary, being a diametrically opposite phenomenon to AIE, aggregation-caused quenching (ACQ) behavior from the same TPE moieties was also reported.[66,67]

However, in general, most of the contrast agents are always "emission on" regardless of their position in or out of tumor sites.[68,69] On the other hand, showing a bit better, the signal of contrast agents can be amplified or quenched once subjected to a target stimuli at diseased areas.[70−72] Although the latter seems to be an optimized strategy, the simplicity of imaging technic may bring about some problems, such as poor signal-to-background ratio. To fill this gap, ratiometric fluorescence-based imaging agents as a robust tool is a major breakthrough for intracellular tracing,[73−78] which has been developed to measure the fluorescence intensity ratio at two different wavelengths, providing a built-in self-correction regardless of the concentration and environmental effects. For example, the TPE-PLGVR$_2$-(PEG$_8$)$_2$-K(PpIX) biosensor constructed by Zhang et al. consisted of a protoporphyrin IX photosensitizer and a TPE molecule using PEGylated Pro-Leu-Gly-Val-Arg peptide sequence as a linker.[73] The overexpressed matrix metalloproteinase-2 (MMP-2) in the tumor region could hydrolyze the PLGVR sequence, leading to the detachment of TPE and PEGylated PpIX. The ratiometric fluorescence ratio between TPE and PpIX could be used to evaluate the MMP-2 expression level, which provided visible and accurate feedback of the photodynamic time and region.

The rapid development of conjugated polymers (CPs) with the desirable functions represents a new research direction and has been widely used for practical applications.[79−88] To date, CPs bearing conjugated double or triple bonds, such as polyacetylenes, polyphenylenes, poly(phenylenevinylene)s, and poly(phenyleneethynylene)s, have been explored and awarded AIE characteristics.[89−92] These functional polymers were mainly synthesized either by polymerization of monomers premodified with AIE-active moieties or by postpolymerization modification strategy, like AIE-active silole-bearing monosubstituted polyacetylene and TPE-containing conjugated polyelectrolytes. Liu et al. reported the design and synthesis of a new far-red/near-infrared CPs with both AIE characteristics and good reactive oxygen species generation ability, which showed bright AIE-active emission and efficient singlet oxygen generation under visible light irradiation for photodynamic cancer cell ablation.[93]

Inspired by the above reports, herein, a new type of amphiphilic block copolymer, P(PFPPI-*co*-TPEPI-*co*-HPPI)-*b*-HPPPI, was synthesized through "one-pot" sequential copolymerization of pentafluorophenyl ester-functionalized phenyl isocyanide monomers (PFPPI; M_1), TPE-functionalized phenyl isocyanide monomers (TPEPI; M_2), and L-hydrophilic phenyl isocyanide monomer (HPPI; M_3) with phenylethynyl Pd(II) complex as a single catalyst in a living manner (Scheme 1).

DOI: 10.1021/acs.macromol.7b00669
Macromolecules 2017, 50, 4114−4125

Scheme 2. Schematic Illustration for the Fabrication of Dye Incorporated Core Cross-Linked (CCL) Complex Micelles and Reducing Agent-Triggered Release as Well as Their Respective Luminescence Behavior[a]

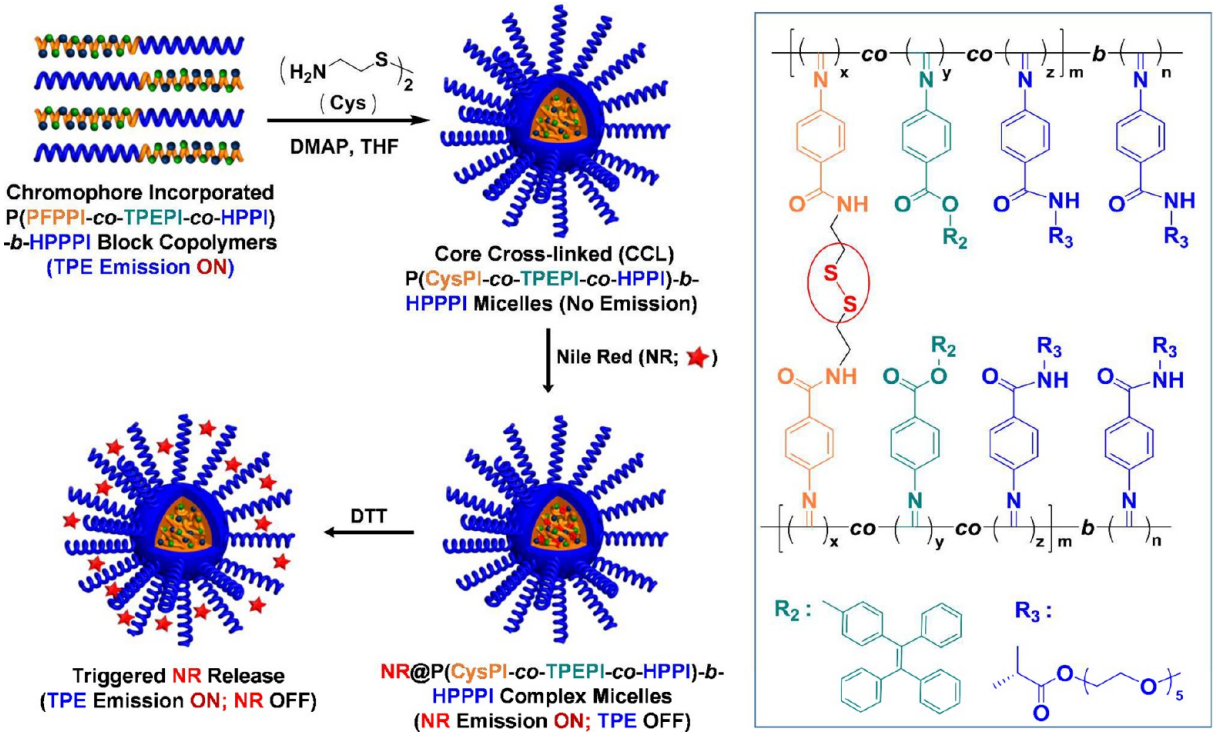

[a]The chemical structure of CCL micelles is shown on the right side.

Table 1. Molecular Parameters of the Polymers Synthesized in This Work

	step 1[a]			step 2[a]		
run	$[M_1]_0/[Cat.]_0$	$[M_2]_0/[Cat.]_0$	$[M_3]_0/[Cat.]_0$	$[M_3]_0/[Cat.]_0$	M_n[b] (kDa)	M_w/M_n[b]
P1[c]	30	10	10		15.5	1.19
P2[d]	30	10	10	50	34.5	1.18
P3[d]	30	20	–	50	32.8	1.16

[a]Initial feed ratio of monomers to catalyst. [b]M_n and M_w/M_n values were determined by SEC analyses with equivalent to polystyrene standard. [c]This sample is isolated from the batch for P2 preparation. [d]These two samples were prepared by a one-pot living polymerization of monomers with a reported phenylethynyl Pd(II).

Then, by utilizing cystamine (Cys) as a cross-linker, the reduction-responsive CCL micelles, P(CysPI-*co*-TPEPI-*co*-HPPI)-*b*-HPPPI, were developed, which showed a time-dependent disruption in the conditions mimicking the intracellular reducing environment and an ACQ optical behavior. To our delight, after incorporating Nile red (NR), the resultant PEGylated single left-handed helical PPI chains surrounded NR@P(CysPI-*co*-TPEPI-*co*-HPPI)-*b*-HPPPI micelles not only possessed rapid cell membrane permeability but also exhibited excellent fluorescence ratiometric cell imaging ability, exposing the real-time disruption of nanocarriers in front of us (Scheme 2). Furthermore, fatal and irreversible damage to cancer cells could be achieved by the high-efficiency delivery of chemotherapeutic agents. Therefore, this newly developed fluorescent integrated nanocarriers allowed stimuli-triggered micelle swelling and imaging as well as further controlled release of the encapsulated drug molecules.

RESULTS AND DISCUSSION

The M_1, M_2, M_3, and phenylethynyl Pd(II) complex were directly used as the same batch in our previously reported literatures.[70,94−97] The well-defined amphiphilic block copolymers, P(PFPPI-*co*-TPEPI-*co*-HPPI)-*b*-HPPPI, with controlled molecular weights (MWs) and tunable compositions were prepared through sequential copolymerization of these three monomers. The copolymerization was catalyzed by phenylethynyl Pd(II) complex in anhydrous THF, and the employed synthetic procedures are described in the Supporting Information Experimental Section and illustrated in Scheme 1. Typically, M_1 (37.5 mg, 0.12 mmol; $[M]_0/[I]_0 = 30$), M_2 (19 mg, 0.04 mmol; $[M]_0/[I]_0 = 10$), and M_3 (18.3 mg, 0.04 mmol; $[M]_0/[I]_0 = 10$) were first copolymerized in the presence of the phenylethynyl Pd(II) complex catalyst (2.0 mg, 0.004 mmol) in anhydrous THF. After the MW of resultant block copolymers (P(PFPPI-*co*-TPEPI-*co*-HPPI); P1 in Table 1) ceased to increase (M_n = 15.5 kDa, M_w/M_n = 1.19; monitored by size-exclusion chromatograms (SEC)), degassed M_3 (91.5 mg, 0.2 mmol; $[M]_0/[I]_0 = 50$) in THF was then added to the reaction mixture via a double-tipped needle. The copolymerization was continued as the second-stage polymerization proceeded. After the copolymerization was completely finished, the final product (P(PFPPI-*co*-TPEPI-*co*-HPPI)-*b*-HPPPI; P2 in Table 1) was collected by precipitation. The chemical structures of P1 and

DOI: 10.1021/acs.macromol.7b00669
Macromolecules 2017, 50, 4114−4125

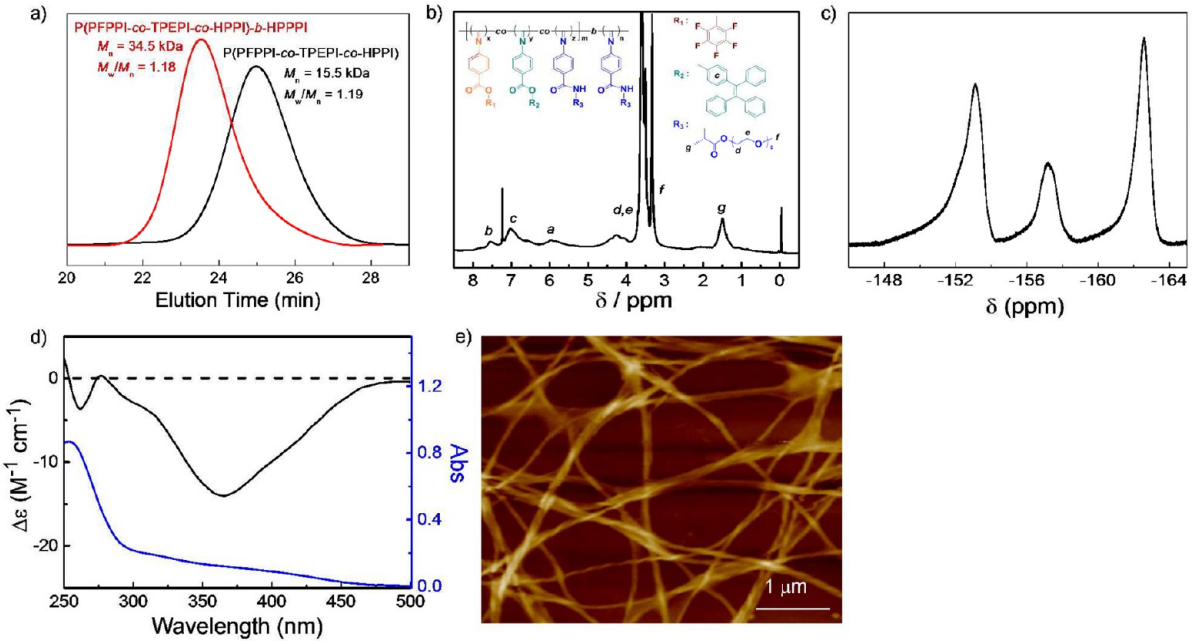

Figure 1. (a) SEC traces obtained for P(PFPPI-*co*-TPEPI-*co*-HPPI) (P1) and P(PFPPI-*co*-TPEPI-*co*- HPPI)-*b*-HPPPI (P2) copolymers, using THF as eluent. (b) ^{1}H and (c) ^{19}F NMR spectra obtained for P2 measured in $CDCl_3$ at 25 °C. (d) CD and UV−vis spectra obtained for P2 in THF at 25 °C. (e) AFM image obtained for P2 dried from THF solution (0.5 g/L).

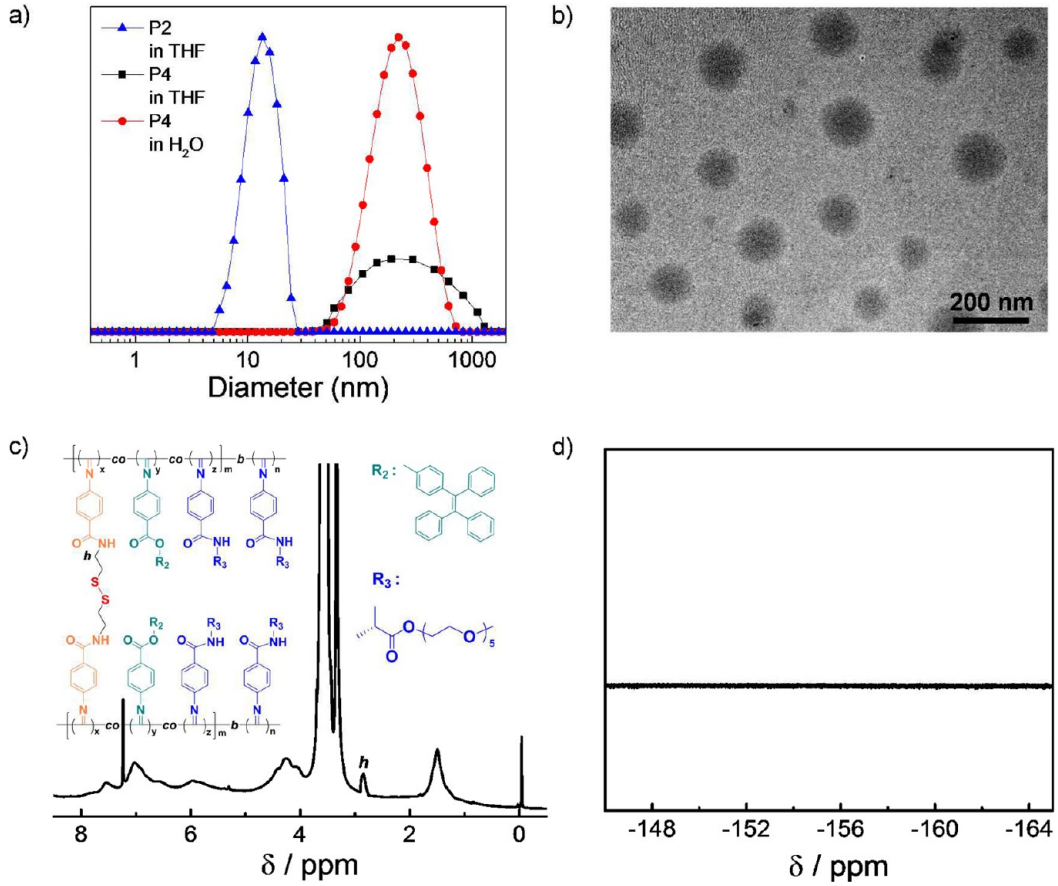

Figure 2. (a) Hydrodynamic diameter distribution of the THF and aqueous dispersions of P2 and cross-linked P4 micelles at 25 °C. (b) TEM image recorded for the morphology of P4 micelles dried from water (0.5 g/L). (c) ^{1}H and (b) ^{19}F NMR spectra obtained for P4 measured in $CDCl_3$ at 25 °C.

P2 were first analyzed by SEC (Figure 1a). Both of them showed single modal elution peaks; P2 with a M_n of 34.5 kDa and M_w/M_n = 1.18 was located in the high-molecular-weight region as compared to P1 (M_n = 15.5 kDa; M_w/M_n = 1.19).

DOI: 10.1021/acs.macromol.7b00669
Macromolecules 2017, 50, 4114−4125

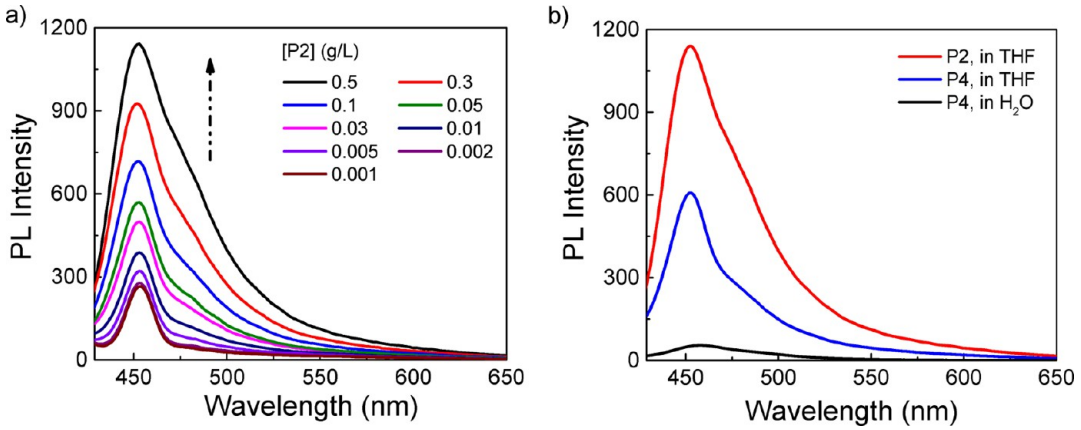

Figure 3. Fluorescence emission spectra (λ_{ex} = 380 nm) recorded for (a) P2 in THF as a function of concentration and (b) the THF and aqueous dispersions of P2 and P4 micelles (0.5 g/L).

The final chemical structure of P2 was further verified by the ^{1}H NMR spectrum (Figure 1b). The proton signals attributed to TPE moieties, PPI blocks, and PEG side chains could be clearly distinguished in the ^{1}H NMR spectrum. Together with the SEC data, the actual degree of polymerization (DP) of P2 could be determined to be P(PFPPI$_{24}$-*co*-TPEPI$_8$-*co*-HPPI$_9$)-*b*-HPPPI$_{42}$. Furthermore, as shown in Figure 1c, the obvious resonance detected in the ^{19}F NMR spectrum suggested the existence of PFP ester residues in the resulting P2 after sequential copolymerization. The FT-IR spectrum of P2 showed a series of intense absorptions coming from the ester linkage, PPI main chains, and the C−F vibrations (Figure S1). On the basis of such a detailed characterization, the expected amphiphilic block copolymers were successfully obtained. For comparison, P(PFPPI-*co*-TPEPI)-*b*-HPPPI without HPPI monomers in the first step (P3 in Table 1) was also prepared in identical feeding ratio with P2. The employed synthetic procedures were the same as P2 and illustrated in Scheme S1. The DP of P3 was also analyzed by SEC (Figure S2). The actual DPs of P3 were determined to be P(PFPPI$_{22}$-*co*-TPEPI$_{16}$)-*b*-HPPPI$_{40}$. The living characters of all the copolymerizations were supported by the accordance between the initial feed ratios of the monomer to catalyst with the final MWs of the afforded polymers. The detailed molecular parameters of P1, P2, and P3 are summarized in Table 1.

Random copolymerization of M_1, M_2, and M_3 afforded the hydrophobic P(PFPPI-*co*-TPEPI-*co*-HPPI) blocks, and the subsequent chain extension by the same M_3 gave a PEGylated single left-handed helical block. It has been confirmed that the copolymerization of PI monomers should give optically active block copolymers, especially for the introduction of L-hydrophilic PPI blocks.[97] Herein, from the circular dichroism (CD) spectrum in Figure 1d, the negative Cotton effect at 364 nm corresponding to the absorption of the n−π^* transition of the C═N of the PPI main chain could be clearly detected with a $\Delta\varepsilon_{364}$ of about −14.8, indicating a single left-handed helical chain was formed. The assembly morphology was obtained by the tapping-mode atomic force microscope (AFM) technique (Figure 1e). Spin-coating of a THF solution (0.5 g/L) of P2 onto a precleaned silicon wafer revealed the well-defined nanofibrils with ca. ∼90−120 nm diameters, and a persistence length of dozens of micrometers was formed. After a careful proofreading, the copolymers were found to self-assemble into single left-handed helical fibrils, which agreed with the CD results and ascribed to the chiral induction ability from L-alanine moieties during the solvent evaporating process.

The activated PFP ester moieties in P2 can be facilely converted to other structures via substitution of them with functional amine or hydroxyl groups; such a method has been successfully applied in the postpolymerization modification.[94,98] In the current study, cystamine (Cys) was used as a cross-linker to fabricate CCL micelles from P2. Dynamic light scattering (DLS) measurements were applied to monitor the cross-linking process. As depicted in Figure 2a, in THF, P2 showed a size distribution of diameter ranging from 6 to 24 nm with a maximum peak value of ∼13.4 nm, implying the existence of its single chains or possible small multimers formed by self-association. Then, after the treatment of Cys ([Cys] = 1/2 [PFP ester]) for 8 h, the mixture showed a distribution at larger and broader diameter ranges (37−1280 nm) with a maximum peak value of ∼240 nm. It should be clarified that the single polymer chains are expected to stay separated, and no aggregates formed if there are no specific interactions. Thus, it is reasonable to consider that Cys plays an important role in forming large cross-linked aggregates, denoted as P(CysPI-*co*-TPEPI-*co*-HPPI)-*b*-HPPPI (P4). To further demonstrate the cross-linking of the core, although a 10-fold volume of THF was added, the micelles maintained their size, and no remarkable change was observed for at least 3 days, indicating the excellent colloidal stability. However, in water, a size distribution of diameter ranging from 60 to 690 nm with maximum peak value of ∼210 nm was obtained. In keeping with the amphiphilic block copolymers, the transmission electron microscope (TEM) image (Figure 2b) revealed spherical nanoparticles with an average size of ∼160 nm were formed in water due to the difference in the solubility between the two parts in a selective solvent. Considering the copolymer compositions, these micelles in water should have cross-linked P(CysPI-*co*-TPEPI-*co*-HPPI) cores and surrounded by a shell of hydrophilic helical PPI chains. The critical association concentration (CAC) is an important parameter to characterize the structural stability of amphiphilic polymeric micelles. Herein, the equilibrium surface tensions were used to determine the CAC values of P1−P4. As shown in Figure S3, all of the surface tension decreased with increasing polymer concentrations, and a change in slope was observed in the curve at a characteristic concentration and then remained approximately constant with further increase of polymer concentration. The CAC values of P1−P4 could be calculated to be

DOI: 10.1021/acs.macromol.7b00669
Macromolecules 2017, 50, 4114−4125

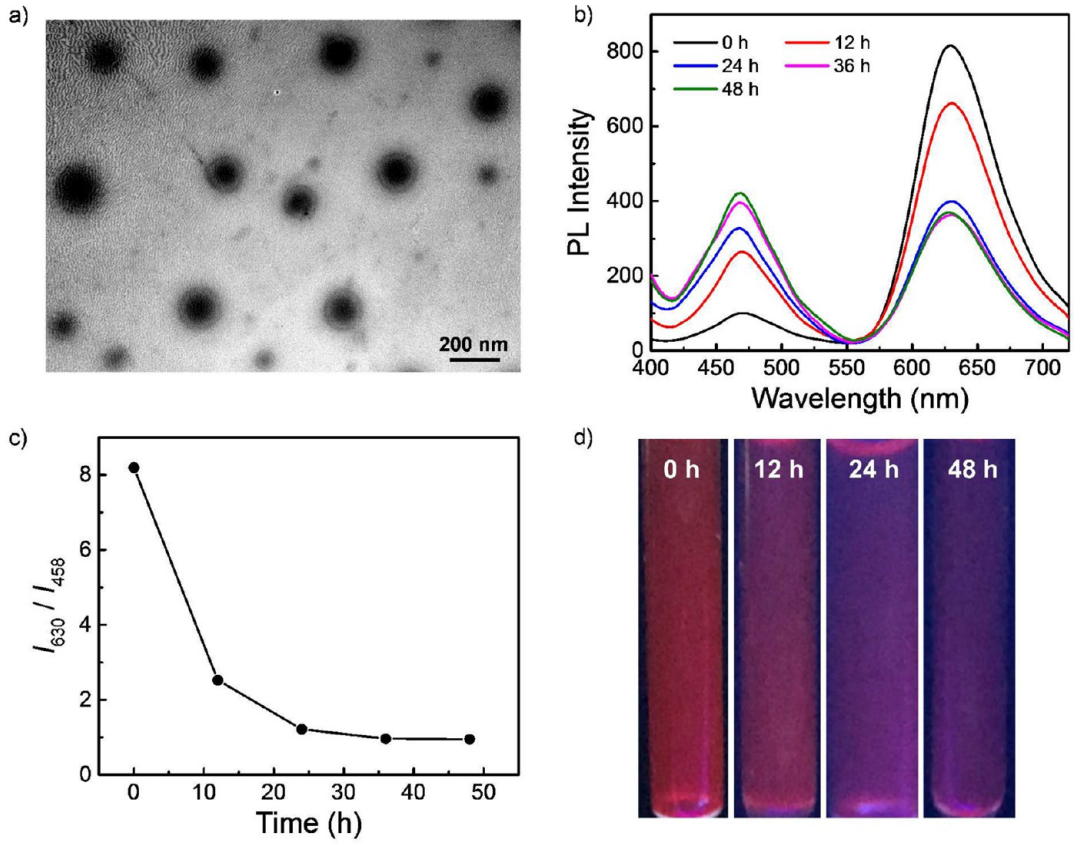

Figure 4. (a) TEM image obtained for the morphology of NR@P4 micelles dried from water (0.2 g/L). (b) Time evolution of fluorescence spectra (λ_{ex} = 380 nm; slit widths: Ex. 5 nm; Em. 5 nm) and (c) time-dependent fluorescence intensity ratio changes, I_{630}/I_{458}, recorded for NR@P4 micellar dispersion (pH 7.4; 0.5 g/L) in the presence of 3.0 mM DTT. (d) Fluorescent photographs taken for the aqueous dispersion of NR@P4 at different times in the same condition under 365 nm UV irradiation from a hand-held UV lamp.

about 0.02, 0.032, 0.054, and 0.0045 g/L, respectively. On the basis of these results, we could conclude that the cross-linked P4 was much more stable in water than P1−P3 because of its lowest CAC value.

The ^{1}H NMR spectrum was further employed to study the extent of core cross-linking. As can be seen from Figure 2c, after core cross-linking, the resonance peaks characteristic of P2 were kept as the original form (Figure 1b). The peak at 2.9 ppm ascribed to the methylene protons of cystamine newly emerged, indicating the high reactivity of the PFP ester toward bifunctional primary amine in cystamine. Additionally, as shown in Figure 2d, no peak was detected in the ^{19}F NMR spectrum of P4, suggesting that no PFP ester residue was contained in the CCL micelles and the pentafluorophenol byproduct was also completely removed during the precipitation.

It had been confirmed by us that TPE-NC monomers and corresponding homopolymers exhibited concentration and molecular weight dependent AIE behavior in pure organic solvents.[95] Differently, TPE-NC monomers maintained AIE activity in the THF/H_2O mixture, but the homopolymers lost their emission in mixed solvent. We ascribed this phenomenon to two possible reasons: (1) the shrinkage in the volume of polymer chains in water brought the phenyl rings closer, which increased their $\pi-\pi$ stacking interactions and quenched the emission; (2) due to the rigid and thermal static helical structure of PPI chains, the local concentration and conformation of TPE units might not be affected by the solvent composition change in the solution and resulted in negligible AIE phenomenon. For P2, although TPE moieties were randomly distributed in the P(PFPPI-*co*-TPEPI-*co*-HPPI) blocks, it still showed obvious concentration-dependent emission in THF solution (Figure 3a). However, they were less fluorescently active once cross-linked structure (P4) was formed, reflecting half of the initial emission intensity of P2 with the same concentration. Furthermore, when P4 was entirely dispersed in pure water, 95% of the emission was quenched as compared with P2 in THF (Figure 3b). Once again, these results verified the different emission behavior between TPE modified conjugated polymers and conventional carbon-chain polymers and are consistent with our previously reported results.

Since Cys was employed to act as the cross-linker, it was connected to the PPI network and concealed within the micelle cores. The disulfide bonds within them can be readily cleaved using a well-known exchange reaction with dithiol compounds such as dithiothreitol (DTT). As expected, the exchange process should accompany the swelling of CCL micelles and result in the inevitable emission change. The time-dependent fluorescent spectra for P4 (0.5 g/L) were recorded in the presence of 3 mM (less than the level of reducing agents in cancer cells) of DTT and depicted in Figure S4a. It showed that the emission intensity of TPE was gradually increased with prolonged times in water, indicating the decreased $\pi-\pi$ stacking interactions between TPE units with the aid of DTT. The change in the relative emission intensity (I_{458}) was then calculated, and an S-shaped curve was obtained (Figure S4b). Such a tendency reflected a slow to fast swelling process

DOI: 10.1021/acs.macromol.7b00669
Macromolecules 2017, 50, 4114−4125

by the gradually increased polarity of the microenvironment due to the cleavage of disulfide bonds to release thiol groups. Not only that the randomly distributed HPPPI chains within the micelle cores also created interconnected hydrophilic channels, which was beneficial for the core to uptake more DTT molecules and led to an enhanced exchange reaction, leading to the more efficient cleavage of disulfide bonds and chain extension of the core and promoting the recovery of TPE emission. Representative fluorescent photographs taken for the aqueous dispersion of P4 at different times in the same condition are displayed in Figure S4c upon UV irradiation at 365 nm. The emission intensity was enhanced according to the time prolonging and agreed well with the fluorescent spectra, which decreased $\pi-\pi$ stacking interactions making the polymer adopted a more twisted structure. Consistently, in THF (Figure S5), the fluorescence intensities were also gradually increased once the incubation time was prolonged from 0 to 24 h. About a 1.88-fold increase was achieved as compared to the initial cross-linked state, which was accordant with the above result (Figure 3b).

DLS was then used to analyze the micelle size change by incubating P4 with DTT. Figure S6a shows the profiles of micelle size distribution before and after incubation with 3 mM DTT for different times in THF. As was seen, treatment with DTT resulted in the broad micelle size distribution moving to the small size range over time and formation of products with significantly smaller size. After incubation for 24 h, the monodispersed profile for single chains (~13.8 nm) illustrated the completely disintegration of P4. In contrast, the size distribution of P4 micelles increased to large-size region from ~210 to ~244 nm after 36 h incubation with DTT in water, confirming the excellent structural stability of cross-linked core and only slight swollen occurred in water (Figure S6b). The integrity of micellar structure in water was brought from the inherent hydrophobicity of the first block in P2, although the indeed enhancement in the microenvironment polarity by DTT treatment. Overall, the above results implied the successful achievement to the dye incorporated and reducing agent responsive nanocarriers.

To explore the reduction-responsive nanocarriers in the field of drug release, solvatochromic Nile red (NR) was encapsulated as a model hydrophobic drug into the CCL P4 micelles to form NR@P4 complex micelles using a cosolvent approach. A typical spherical morphology of NR@P4 was obtained by the TEM technique (Figure 4a), revealing a much larger size and more apparent contrast of core−shell structure than that of P4 micelles (Figure 2b), which should be ascribed to the encapsulation of NR molecules in the cores. Then, the quantitative relationship between the released NR and DTT treating time was investigated by the fluorescence spectrum (Figure S7). In the absence of DTT, the fluorescence intensity of NR remained unchanged, suggesting the stable micellar structure with NR encapsulated in the hydrophobic cores. Then, after the addition of 3 mM DTT, the fluorescence intensity (I_{630}) of NR gradually decreased (Figure S7a), indicating the occurrence of micelle swollen and resulting in the NR release by cleavage of the disulfide cross-linker. The percent of NR released from NR@P4 micelles was approximately 56% after 36 h incubation with 3 mM DTT, and a local plateau was observed thereafter (Figure S7b), indicating the capability of stimuli-triggered cargo release. As we know, DTT is a much better thiol reducing agent than glutathione (GSH). Thus, the fluorescence emission spectra recorded for the aqueous dispersion of NR@P4 micelles (0.5 g/L) at different times in the presence of 3 mM GSH were performed to mimic the reduction environment in cells. From Figure S7c,d, similar emission spectra and release curves as well as corresponding tendency were obtained in the presence of GSH as compared with DTT. Although DTT is a much better thiol reducing agent than GSH in general, the existence of randomly distributed hydrophilic PPI chains within micelle cores created interconnected hydrophilic channels, which was beneficial for the core to facilely uptake more GSH molecules and enhance the exchange reaction, leading to the more efficient cleavage of disulfide bonds. This ingenious design avoids the property difference between DTT and GSH.

Thanks to the different optical properties of TPE and NR in the same nanocarrier, a ratiometric emission behavior can be constructed. From Figure 4b, we could apparently distinguish two emission peaks at around 630 and 458 nm, which were ascribed to the emissions from NR and TPE, respectively. With the treatment of DTT, the high-wavelength fluorescence signal (I_{630}) observably decreased with incubation time, indicating the release of NR. At the same time, the low-wavelength fluorescence signal (I_{458}) from TPE gradually increased, revealing the relaxation of original compact micellar structures and more twisted TPE moieties. The time-dependent fluorescence intensity ratio (I_{630}/I_{458}) is depicted in Figure 4c; an almost 9-fold decrease was acquired in the experimental time range, reflecting a more apparent change as compared to single chromophore contained samples (Figures S4 and S7). Compared with P4, the control sample (NR@P3) without HPPI moieties in the first block showed slight intensity change for both of TPE and NR (Figure S8), indicating the strong resistance in the cleavage of disulfide bonds due to the lack of interconnected hydrophilic channels brought by randomly distributed HPPI in the cores. Nevertheless, the DTT-induced fluorescence ratiometric changes could also be visualized by the naked eye, as evidenced from the color transition from red to violet (mixture of red and blue color) emission after treatment by DTT (Figure 4c).

The successful ratiometric expression of NR@P4 micelles in vitro encouraged us to examine whether they could work in living cells. As reported in our previous literatures,[70,97] PEGylated single left-handed helical PPI corona endowed relevant polymeric nanocarrier rapid cell membrane permeability that had analogous effect of cell penetrating peptides (CPPs) and poly(arginine) mimics as reported by Cheng et al.[99] The cell membrane permeability of NR@P4 micelles was studied and observed by a confocal laser scanning microscope (CLSM). As expected, upon being co-incubated with HeLa cells at 37 °C, the intracellular red emission could be observed indistinctly after a short time range and tended to be much brighter and clearer at 40 min; the whole endocytosis process took about 120 min (Figure S9). Apparently, a much slower process appeared in the current situation than that of our previously reported time range (1 h).[70,97] The prolongation of time scales for NR@P4 micelles here was owing to the much bigger micellar size because of the larger MWs as well as the introduction of hydrophilic PPI chains in the micelle cores, which lowered the hydrophobicity of inner core more or less. Anyway, benefiting from the single left-handed PPI chains, it was indeed an order of magnitude improvement of penetrating rate compared to other polymeric nanocarriers.[70]

The imaging performance of NR@P4 micelles was subsequently investigated. As shown in the CLSM images

DOI: 10.1021/acs.macromol.7b00669
Macromolecules 2017, 50, 4114−4125

from Figure 5, the red fluorescence emission in cells from NR channel observably decreased with time from 2 to 36 h, but it

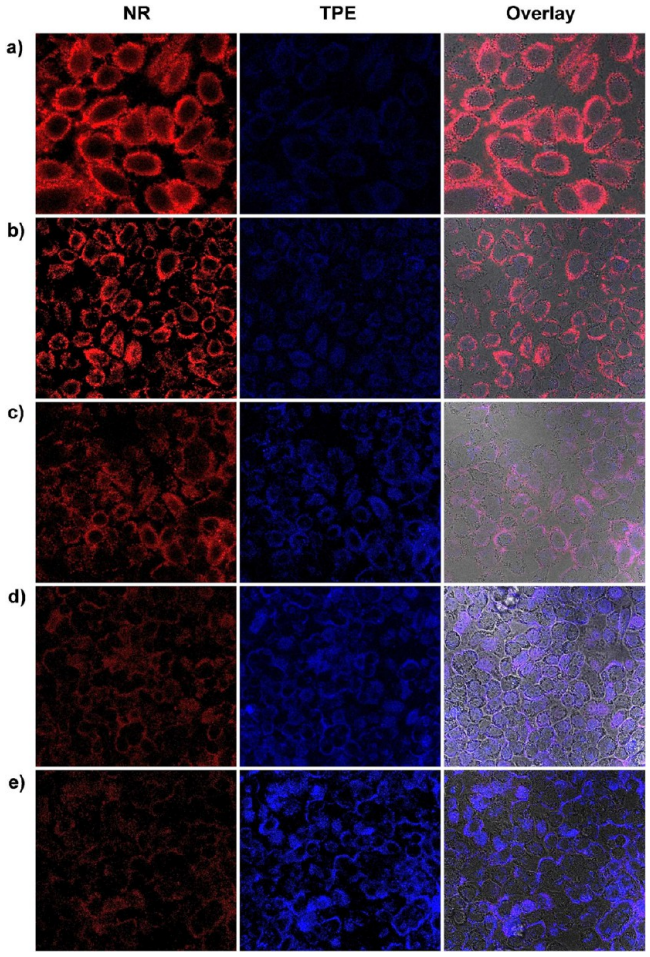

Figure 5. Incubation duration-dependent CLSM images of live HeLa cells when culturing at 37 °C with NR@P4 micelles (0.3 g/L): (a) 2, (b) 6, (c) 12, (d) 24, and (e) 36 h. The red channel for NR was excited at 550 nm and collected between 580 and 700 nm, and the blue channel for TPE was excited at 405 nm and collected between 410 and 500 nm.

was still measurable owing to the incomplete release of incorporated NR molecules within the micelle core, which agreed well with the in vitro release profile (Figure S7). However, at the same time, the blue fluorescence emission from TPE channel gradually increased in the same time scale and finally occupied the dominant position in cells. The change in the ratio of emission intensity (overlay column) showed a color transition from red to purple to blue, confirming the successful development of a chiral polymeric nanoparticle based ratiometric probes to realize the cancer cell microenvironment responsive detection. The typical magnification of CLSM images of live HeLa cells when culturing at 37 °C with NR@P4 micelles (0.3 g/L) for 12 h is provided in the Supporting Information (Figure S10).

Finally, the anticancer drug camptothecin (CPT) was embedded in the P4 micelles to form CPT@P4 complex micelles. The CPT encapsulation efficiency and loading content were calculated to be ~64.1% w/w and ~6.02% w/w based on the absorbance of CPT at 355 nm against standard calibration curves. First, the in vitro dose-dependent cytotoxicity of pure P4, NR@P4, and CPT@P4 was systematically investigated by MTT assay. After incubating HeLa cells with different concentrations of these micelles for 12 h, Figure 6 clearly

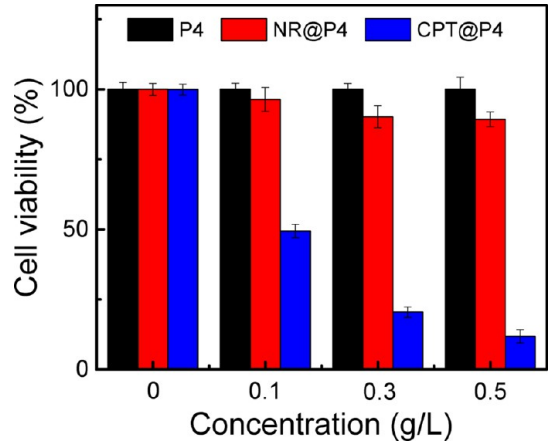

Figure 6. Viability of HeLa cells after being incubated with pure P4, NR@P4, and CPT@P4 micelles with various concentrations for 12 h. The error bars are based on the standard deviations of four parallel samples.

shows that pure P4 had negligible cytotoxicity on cancer cells. For the NR@P4, a slight cytotoxicity (~10% cell death) was observed at high micelle concentrations (0.5 g/L). However, the CPT@P4 micelles exhibited a remarkable cytotoxicity, killing about 80% and 89% cells at micelle concentration of 0.3 and 0.5 g/L, respectively. This result indicated that the CPT loaded micelles had an excellent chemotherapy effect on cancer cells, while the polymeric nanocarriers and NR dyes had a slight influence on cell viability.

Moreover, the in vitro cytotoxicity assessments could also be directly observed by calcein-AM and propidium idodide (PI) staining. The live cells were stained with calcein-AM, and dead cells were stained with PI. Cells incubated without any additives were served as positive control. For comparison, the cytotoxicity of blank control, P4 micelles, and CPT@P4 micelles was assessed following the same procedures. The cell death percentage was calculated by the ratio of corresponding fluorescence intensity (red/green). After incubating HeLa cells with CPT@P4 micelles (0.3 g/L), Figure 7a clearly shows that ~82% of the cells were killed by CPT@P4 micelles after 12 h incubation, whereas more than 95% of the cells kept active after treating with pure P4 under the same conditions, as evidenced by the presence of few dead cells (red points) in Figure 7b. Furthermore, the blank control without any additives exhibited no influence on the cells activity (Figure 7c). These results confirmed that the pure P4 micelles have negligible toxicity on cancer cells, and the crucial role played by the anticancer drug was ascertained.

CONCLUSION

In summary, a new type of TPE embedded amphiphilic block copolymer, P(PFPPI-*co*-TPEPI-*co*-HPPI)-*b*-HPPPI, was prepared through a "one-pot" sequential living copolymerization of three different functional groups substituted PI monomers. Exchange reaction between PFP units and Cys was employed to achieve core cross-linking, which not only improved the structural stability of the micelles but also allowed controlled release of cargo molecules in response to the reducing

DOI: 10.1021/acs.macromol.7b00669
Macromolecules 2017, 50, 4114−4125

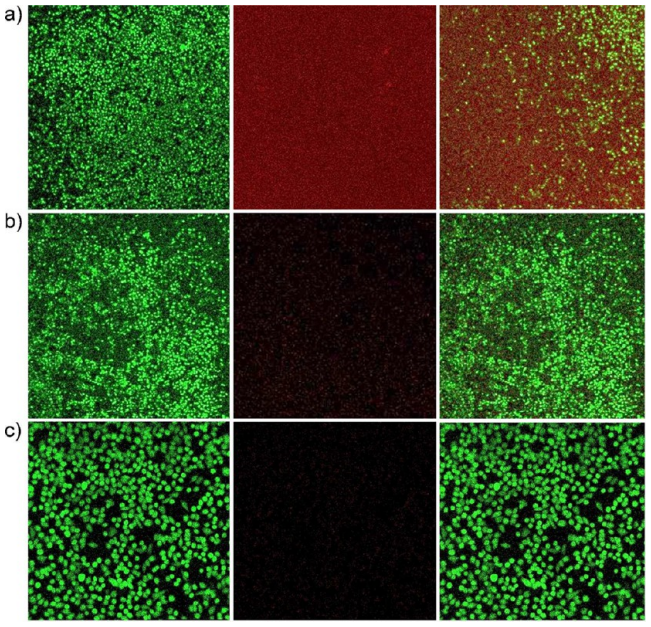

Figure 7. Fluorescence images of calcein AM/PI costained HeLa cells after incubation with CPT@P4 micelles (0.3 g/L) for 12 h (a). Cells incubated with the same concentration of pure P4 micelles without CPT (b) and blank (c) were chosen as controls.

environment. After NR dyes were incorporated, the fluorescence ratiometric behavior of NR@P4 micelles endowed them excellent cell imaging ability and provided an accurate dissociation process of internalized micelles. Moreover, the PEGylated single left-handed helical polymer coronas played an important role to guide these nanocarriers into cancer cells that had an analogous effect of cell penetrating peptides (CPPs). This work opens a new direction toward the construction of smart drug delivery systems capable of fluorescence ratiometric behavior simultaneously and has a broad application prospects.

■ ASSOCIATED CONTENT

Supporting Information

The Supporting Information is available free of charge on the ACS Publications website at DOI: 10.1021/acs.macromol.7b00669.

Additional FT-IR, fluorescent spectra, hydrodynamic diameter distribution, and other characterization data (PDF)

■ AUTHOR INFORMATION

Corresponding Author

*E-mail: yinjun@hfut.edu.cn (J.Y.).

ORCID

Jun Yin: 0000-0001-8641-3209

Zong-Quan Wu: 0000-0001-6657-9316

Author Contributions

X.H. and J.Z. contributed equally to this work.

Notes

The authors declare no competing financial interest.

■ ACKNOWLEDGMENTS

This work was supported by National Natural Scientific Foundation of China (51673058). Z.W. thanks the Thousand Young Talents Program for financial support.

■ REFERENCES

(1) Ge, Z. S.; Liu, S. Y. Functional block copolymer assemblies responsive to tumor and intracellular microenvironments for site-specific drug delivery and enhanced imaging performance. *Chem. Soc. Rev.* **2013**, *42*, 7289−7325.

(2) Sheng, Z. H.; Hu, D. H.; Xue, M. M.; He, M.; Gong, P.; Cai, L. T. Indocyanine green nanoparticles for theranostic applications. *Nano-Micro Lett.* **2013**, *5*, 145−150.

(3) Jokerst, J. V.; Gambhir, S. S. Molecular imaging with theranostic nanoparticles. *Acc. Chem. Res.* **2011**, *44*, 1050−1060.

(4) Funkhouser, J. Reinventing pharma: the theranostic revolution. *Curr. Drug Discovery* **2002**, *2*, 17−19.

(5) Kamaly, N.; Xiao, Z.; Valencia, P. M.; Radovic-Moreno, A. F.; Farokhzad, O. C. Targeted polymeric therapeutic nanoparticles: design, development and clinical translation. *Chem. Soc. Rev.* **2012**, *41*, 2971−3010.

(6) Yang, K.; Xu, H.; Cheng, L.; Sun, C. Y.; Wang, J.; Liu, Z. *Adv. Mater.* **2012**, *24*, 5586−5592.

(7) Fan, Q. L.; Cheng, K.; Yang, Z.; Zhang, R. P.; Yang, M.; Hu, X.; Ma, X. W.; Bu, L. H.; Lu, X. M.; Xiong, X. X.; Huang, W.; Zhao, H.; Cheng, Z. *Adv. Mater.* **2015**, *27*, 843−847.

(8) Deng, Z. Y.; Qian, Y. F.; Yu, Y. Q.; Liu, G. H.; Hu, J. M.; Zhang, G. Y.; Liu, S. Y. Engineering intracellular delivery nanocarriers and nanoreactors from oxidation-responsive polymersomes via synchronized bilayer crosslinking and permeabilizing inside live cells. *J. Am. Chem. Soc.* **2016**, *138*, 10452−10466.

(9) Li, Y. M.; Liu, G. H.; Wang, X. R.; Hu, J. M.; Liu, S. Y. Enzyme-responsive polymeric vesicles for bacterialstrain-selective delivery of antimicrobial agents. *Angew. Chem., Int. Ed.* **2016**, *55*, 1760−1764.

(10) Wang, X. R.; Hu, J. M.; Liu, G. H.; Tian, J.; Wang, H. J.; Gong, M.; Liu, S. Y. Reversibly switching bilayer permeability and release modules of photochromic polymersomes stabilized by cooperative noncovalent interactions. *J. Am. Chem. Soc.* **2015**, *137*, 15262−15275.

(11) Liu, G. H.; Zhang, G. F.; Hu, J. M.; Wang, X. R.; Zhu, M. Q.; Liu, S. Y. Hyperbranched self-immolative polymers (hSIPs) for programmed payload delivery and ultrasensitive detection. *J. Am. Chem. Soc.* **2015**, *137*, 11645−11655.

(12) Hu, X. L.; Liu, G. H.; Li, Y.; Wang, X. R.; Liu, S. Y. Cell-penetrating hyperbranched polyprodrug amphiphiles for synergistic reductive milieu-triggered drug release and enhanced magnetic resonance signals. *J. Am. Chem. Soc.* **2015**, *137*, 362−368.

(13) Hu, J. M.; Zhang, G. Q.; Liu, S. Y. Enzyme-responsive polymeric assemblies, nanoparticles and hydrogels. *Chem. Soc. Rev.* **2012**, *41*, 5933−5949.

(14) Hu, C. M.; Fang, R. H.; Luk, B. T.; Zhang, L. Polymeric nanotherapeutics: clinical development and advances in stealth functionalization strategies. *Nanoscale* **2014**, *6*, 65−75.

(15) Koo, A. N.; Lee, H. J.; Kim, S. E.; Chang, J. H.; Park, C.; Kim, C.; Park, J. H.; Lee, S. C. Disulfide-cross-linked PEG-poly(amino acid)s copolymer micelles for glutathione-mediated intracellular drug delivery. *Chem. Commun.* **2008**, 6570−6572.

(16) Rijcken, C. J.; Snel, C. J.; Schiffelers, R. M.; Van Nostrum, C. F.; Hennink, W. E. Hydrolysable core-crosslinked thermosensitive polymeric micelles: synthesis, characterisation and *in vivo* studies. *Biomaterials* **2007**, *28*, 5581−5593.

(17) Guo, A.; Liu, G.; Tao, J. Star polymers and nanospheres from cross-linkable diblock copolymers. *Macromolecules* **1996**, *29*, 2487−2493.

(18) Jiang, X. Z.; Liu, S. Y.; Narain, R. Degradable thermoresponsive core cross linked micelles: fabrication, surface functionalization, and biorecognition. *Langmuir* **2009**, *25*, 13344−13350.

(19) Jiang, X. Z.; Zhang, J. Y.; Zhou, Y. M.; Xu, J.; Liu, S. Y. Facile preparation of core-crosslinked micelles from azide-containing thermoresponsive double hydrophilic diblock copolymer via click chemistry. *J. Polym. Sci., Part A: Polym. Chem.* **2008**, *46*, 860−871.

(20) O'Reilly, R. K.; Joralemon, M. J.; Hawker, C. J.; Wooley, K. L. Preparation of orthogonally-functionalized core click cross-linked nanoparticles. *New J. Chem.* **2007**, *31*, 718−724.

DOI: 10.1021/acs.macromol.7b00669
Macromolecules 2017, 50, 4114−4125

(21) Kakizawa, Y.; Harada, A.; Kataoka, K. Environment-sensitive stabilization of core-shell structured polyion complex micelle by reversible cross-linking of the core through disulfide bond. *J. Am. Chem. Soc.* **1999**, *121*, 11247−11248.
(22) Kim, J. O.; Sahay, G.; Kabanov, A. V.; Bronich, T. K. Polymeric micelles with ionic cores containing biodegradable cross-links for delivery of chemotherapeutic agents. *Biomacromolecules* **2010**, *11*, 919−926.
(23) Wu, Z.; Huang, J. B.; Yan, Y. Electrostatic polyion micelles with fluorescence and MRI dual functions. *Langmuir* **2015**, *31*, 7926−7933.
(24) Huynh, V. T.; Chen, G. J.; de Souza, P.; Stenzel, M. H. Thiol-yne and thiol-ene "click" chemistry as a tool for a variety of platinum drug delivery carriers, from statistical copolymers to crosslinked micelles. *Biomacromolecules* **2011**, *12*, 1738−1751.
(25) Wiltshire, J. T.; Qiao, G. G. Selectively degradable core cross-linked star polymers. *Macromolecules* **2006**, *39*, 9018−9027.
(26) Piogé, S.; Nesterenko, A.; Brotons, G.; Pascual, S.; Fontaine, L.; Gaillard, C.; Nicol, E. Core cross-linking of dynamic diblock copolymer micelles: quantitative study of photopolymerization efficiency and micelle structure. *Macromolecules* **2011**, *44*, 594−603.
(27) Kuckling, D.; Vo, C. D.; Wohlrab, S. E. Preparation of nanogels with temperature-responsive core and pH-responsive arms by photo-cross-linking. *Langmuir* **2002**, *18*, 4263−4269.
(28) Zhang, Z. H.; Yin, L. C.; Tu, C. L.; Song, Z. Y.; Zhang, Y. F.; Xu, Y. X.; Tong, R.; Zhou, Q.; Ren, J.; Cheng, J. J. Redox-responsive, core cross-linked polyester micelles. *ACS Macro Lett.* **2013**, *2*, 40−44.
(29) Wang, Y. H.; Zheng, M.; Meng, F. H.; Zhang, J.; Peng, R.; Zhong, Z. Y. Branched polyethylenimine derivatives with reductively cleavable periphery for safe and efficient *in vitro* gene transfer. *Biomacromolecules* **2011**, *12*, 1032−1040.
(30) Wang, X. X.; Zhang, J.; Cheng, R.; Meng, F. H.; Deng, C.; Zhong, Z. Y. Facile synthesis of reductively degradable biopolymers using cystamine diisocyanate as a coupling agent. *Biomacromolecules* **2016**, *17*, 882−890.
(31) Wang, Y.; Nie, J. S.; Chang, B. S.; Sun, Y. F.; Yang, W. L. Poly(vinylcaprolactam)-based biodegradable multiresponsive microgels for drug delivery. *Biomacromolecules* **2013**, *14*, 3034−3046.
(32) Wan, X. J.; Wang, D.; Liu, S. Y. Fluorescent pH-sensing organic/inorganic hybrid mesoporous silica nanoparticles with tunable redox-responsive release capability. *Langmuir* **2010**, *26*, 15574−15579.
(33) Wang, L.; Zhang, L.; Zhang, X. B.; Wei, X.; Tang, Z. M.; Zhou, S. B. Precise polymerization of a highly tumor microenvironment-responsive nanoplatform for strongly enhanced intracellular drug release. *ACS Appl. Mater. Interfaces* **2016**, *8*, 5833−5846.
(34) Poh, P.; Lin, J. B.; Panitch, A. Release of Anti-inflammatory peptides from thermosensitive nanoparticles with degradable cross-links suppresses pro-inflammatory cytokine production. *Biomacromolecules* **2015**, *16*, 1191−1200.
(35) Zhou, K. Y.; Cao, H.; Gao, P.; Cui, Z. G.; Ding, Y.; Cai, Y. L. Autocatalytic self-sorting in biomimetic polymer. *Macromolecules* **2016**, *49*, 2189−2196.
(36) Cheng, R.; Feng, F.; Meng, F. H.; Deng, C.; Feijen, J.; Zhong, Z. Y. Glutathione-responsive nano-vehicles as a promising platform for targeted intracellular drug and gene delivery. *J. Controlled Release* **2011**, *152*, 2−12.
(37) Schafer, F. Q.; Buettner, G. R. Redox environment of the cell as viewed through the redox state of the glutathione disulfide/glutathione couple. *Free Radical Biol. Med.* **2001**, *30*, 1191−1212.
(38) Wei, T.; Liu, J.; Ma, H.; Cheng, Q.; Huang, Y.; Zhao, J.; Huo, S.; Xue, X.; Liang, Z.; Liang, X. J. Functionalized nanoscale micelles improve drug delivery for cancer therapy *in vitro* and *in vivo*. *Nano Lett.* **2013**, *13*, 2528−2534.
(39) Wang, Y.; Zhou, K.; Huang, G.; Hensley, C.; Huang, X.; Ma, X.; Zhao, T.; Sumer, B. D.; DeBerardinis, R. J.; Gao, J. A nanoparticle-based strategy for the imaging of a broad range of tumors by nonlinear amplification of microenvironment signals. *Nat. Mater.* **2013**, *13*, 204−212.
(40) Wu, X.; Sun, X.; Guo, Z.; Tang, J.; Shen, Y.; James, T. D.; Tian, H.; Zhu, W. In vivo and in situ tracking cancer chemotherapy by highly photostable NIR fluorescent theranostic prodrug. *J. Am. Chem. Soc.* **2014**, *136*, 3579−3588.
(41) Chen, Y. J.; Han, H. J.; Tong, H. X.; Chen, T. T.; Wang, H. B.; Ji, J.; Jin, Q. Zwitterionic phosphorylcholine-TPE conjugate for pH-responsive drug delivery and AIE active imaging. *ACS Appl. Mater. Interfaces* **2016**, *8*, 21185−21192.
(42) Xue, X. D.; Jin, S. B.; Zhang, C. Q.; Yang, K. N.; Huo, S. H.; Chen, F.; Zou, G. Z.; Liang, X. J. Probe-inspired nano-prodrug with dual-color fluorogenic property reveals spatiotemporal drug release in living cells. *ACS Nano* **2015**, *9*, 2729−2739.
(43) Li, Y.; Shao, A.; Wang, Y.; Mei, J.; Niu, D.; Gu, J.; Shi, P.; Zhu, W.; Tian, H.; Shi, J. Morphology-tailoring of a red AIEgen from microsized rods to nanospheres for tumor-targeted bioimaging. *Adv. Mater.* **2016**, *28*, 3187−3193.
(44) Wan, Q.; Wang, K.; He, C.; Liu, M.; Zeng, G.; Huang, H.; Deng, F.; Zhang, X.; Wei, Y. Stimulus responsive cross-linked AIE-active polymeric nanoprobes: fabrication and biological imaging application. *Polym. Chem.* **2015**, *6*, 8214−8221.
(45) Ma, H.; Qi, C.; Cheng, C.; Yang, Z.; Cao, H.; Yang, Z.; Tong, J.; Yao, X.; Lei, Z. AIE-active tetraphenylethylene cross-linked NIsopropylacrylamide polymer: A long-term fluorescent cellular tracker. *ACS Appl. Mater. Interfaces* **2016**, *8*, 8341−8348.
(46) Dong, Y. Q.; Lam, J. W. Y.; Qin, A.; Sun, J. X.; Liu, J.; Li, Z.; Zhang, S.; Sun, J. Z.; Kwok, H. S.; Tang, B. Z. Aggregation-induced emissions of tetraphenylethene derivatives and their utilities as chemical vapor sensors and in organic light-emitting diodes. *Appl. Phys. Lett.* **2007**, *91*, 011111−1−011111−3.
(47) Luo, J.; Xie, Z.; Lam, J. W. Y.; Cheng, L.; Tang, B. Z.; Chen, H.; Qiu, C.; Kwok, H. S.; Zhan, X.; Liu, Y.; Zhu, D. Aggregation-induced emission of 1-methyl-1,2,3,4,5-pentaphenylsilole. *Chem. Commun.* **2001**, 1740−1741.
(48) Yu, Y.; Feng, C.; Hong, Y.; Liu, J.; Chen, S.; Ng, K. M.; Luo, K. Q.; Tang, B. Z. Cytophilicfluorescent bioprobes for long-term cell tracking. *Adv. Mater.* **2011**, *23*, 3298−3302.
(49) Li, Z.; Dong, Y. Q.; Lam, J. W.; Sun, J.; Qin, A.; Häußler, M.; Dong, Y. P.; Sung, H. H.; Williams, I. D.; Kwok, H. S.; Tang, B. Z. Functionalized siloles: versatile synthesis, aggregation-induced emission, and sensory and device applications. *Adv. Funct. Mater.* **2009**, *19*, 905−917.
(50) Wang, Z.; Yong, T. Y.; Wan, J. S.; Li, Z. H.; Zhao, H.; Zhao, Y. B.; Gan, L.; Yang, X. Y.; Xu, H. B.; Zhang, C. Temperature-sensitive fluorescent organic nanoparticles with aggregation-induced emission for long-term cellular tracing. *ACS Appl. Mater. Interfaces* **2015**, *7*, 3420−3425.
(51) Jiang, B. P.; Tan, X. Y.; Shen, X. C.; Lei, W. Q.; Liang, W. Q.; Ji, S. C.; Liang, H. One-step fabrication of a multifunctional aggregation-induced emission nanoaggregate for targeted cell imaging and enzyme-triggered cancer chemotherapy. *ACS Macro Lett.* **2016**, *5*, 450−454.
(52) Wang, X.; Yang, Y. Y.; Zhuang, Y. P.; Gao, P. Y.; Yang, F.; Shen, H.; Guo, H. X.; Wu, D. C. Fabrication of pH-responsive nanoparticles with an AIE feature for imaging intracellular drug delivery. *Biomacromolecules* **2016**, *17*, 2920−2929.
(53) Shi, H. B.; Kwok, R. T. K.; Liu, J. Z.; Xing, B. G.; Tang, B. Z.; Liu, B. Real-time monitoring of cell apoptosis and drug screening using fluorescent light-up probe with aggregation-induced emission characteristics. *J. Am. Chem. Soc.* **2012**, *134*, 17972−17981.
(54) Jiang, B. P.; Guo, D. S.; Liu, Y. C.; Wang, K. P.; Liu, Y. Photomodulated fluorescence of supramolecular assemblies of sulfonatocalixarenes and tetraphenylethene. *ACS Nano* **2014**, *8*, 1609−1618.
(55) Zhang, X.; Yang, Z.; Chi, Z.; Chen, M.; Xu, B.; Wang, C.; Liu, S.; Zhang, Y.; Xu, J. R. A multi-sensing fluorescent compound derived from cyanoacrylic acid. *J. Mater. Chem.* **2010**, *20*, 292−298.
(56) Zhang, X.; Chi, Z.; Xu, B.; Li, H.; Yang, Z.; Li, X.; Liu, S.; Zhang, Y.; Xu, J. R. Synthesis of blue light emitting bis(triphenylethylene) derivatives: A case of aggregation-induced emission enhancement. *Dyes Pigm.* **2011**, *89*, 56−62.
(57) Zhang, X.; Chi, Z.; Xu, B.; Li, H.; Zhou, W.; Li, X.; Zhang, Y.; Liu, S.; Xu, J. R. Comparison of responsive behaviors of two cinnamic

DOI: 10.1021/acs.macromol.7b00669
Macromolecules 2017, 50, 4114−4125

acid derivatives containing carbazolyl triphenylethylene. *J. Fluoresc.* **2011**, *21*, 133−140.
(58) Zhang, X.; Chi, Z.; Xu, B.; Chen, C.; Zhou, X.; Zhang, Y.; Liu, S.; Xu, J. R. End-group effects of piezofluorochromic aggregation-induced enhanced emission compounds containing distyrylanthracene. *J. Mater. Chem.* **2012**, *22*, 18505−18513.
(59) Zhang, X.; Chi, Z.; Zhang, J.; Li, H.; Xu, B.; Li, X.; Liu, S.; Zhang, Y.; Xu, J. R. Piezofluorochromic properties and mechanism of an aggregation-induced emission enhancement compound containing N-Hexyl-phenothiazine and anthracene moieties. *J. Phys. Chem. B* **2011**, *115*, 7606−7611.
(60) Zhang, X.; Chi, Z.; Zhou, X.; Liu, S.; Zhang, Y.; Xu, J. R. Influence of carbazolyl groups on properties of piezofluorochromic aggregation-enhanced emission compounds containing distyrylanthracene. *J. Phys. Chem. C* **2012**, *116*, 23629−23638.
(61) Zhang, X.; Chi, Z.; Xu, B.; Jiang, L.; Zhou, X.; Zhang, Y.; Liu, S.; Xu, J. R. Multifunctional organic fluorescent materials derived from 9,10-distyrylanthracene with alkoxyl endgroups of various lengths. *Chem. Commun.* **2012**, *48*, 10895−10897.
(62) Wang, Z. K.; Chen, S. J.; Lam, J. W. Y.; Qin, W.; Kwok, R. T. K.; Xie, N.; Hu, Q. L.; Tang, B. Z. Long-term fluorescent cellular tracing by the aggregates of AIE bioconjugates. *J. Am. Chem. Soc.* **2013**, *135*, 8238−8245.
(63) Zhang, X. Y.; Zhang, X. Q.; Yang, B.; Liu, M. Y.; Liu, W. Y.; Chen, Y. W.; Wei, Y. Polymerizable aggregation-induced emission dye-based fluorescent nanoparticles for cell imaging applications. *Polym. Chem.* **2014**, *5*, 356−360.
(64) Wang, K.; Zhang, X.; Zhang, X.; Ma, C.; Li, Z.; Huang, Z.; Zhang, Q.; Wei, Y. Preparation of emissive glucose-containing polymer nanoparticles and their cell imaging applications. *Polym. Chem.* **2015**, *6*, 4455−4461.
(65) Huang, Z.; Zhang, X.; Zhang, X.; Fu, C.; Wang, K.; Yuan, J.; Tao, L.; Wei, Y. Amphiphilic fluorescent copolymers *via* one-pot combination of chemoenzymatic transesterification and RAFT polymerization: synthesis, self-assembly and cell imaging. *Polym. Chem.* **2015**, *6*, 607−612.
(66) Chan, C. Y. K.; Lam, J. W. Y.; Deng, C.; Chen, X.; Wong, K. S.; Tang, B. Z. Synthesis, light emission, explosive detection, fluorescent photopatterning, and optical limiting of disubstituted polyacetylenes carrying tetraphenylethene luminogens. *Macromolecules* **2015**, *48*, 1038−1047.
(67) He, Y. G.; Shi, S. Y.; Liu, N.; Ding, Y. S.; Yin, J.; Wu, Z. Q. Tetraphenylethene-functionalized conjugated helical poly(phenyl isocyanide) with tunable light emission, assembly morphology, and specific applications. *Macromolecules* **2016**, *49*, 48−58.
(68) Kobayashi, H.; Choyke, P. L. Target-cancer-cell-specific activatable fluorescence imaging probes: rational design and *in vivo* applications. *Acc. Chem. Res.* **2011**, *44*, 83−90.
(69) Viger, M. L.; Sankaranarayanan, J.; de Gracia Lux, C.; Chan, M.; Almutairi, A. Collective activation of MRI agents via encapsulation and disease-triggered release. *J. Am. Chem. Soc.* **2013**, *135*, 7847−7850.
(70) Shi, S. Y.; Liu, Y. J.; Chen, Y.; Zhang, Z. H.; Ding, Y. S.; Wu, Z. Q.; Yin, J.; Nie, L. M. Versatile pH-response micelles with high cell-penetrating helical diblock copolymers for photoacoustic imaging guided synergistic chemo-photothermal therapy. *Theranostics* **2016**, *6*, 2170−2182.
(71) Lindner, U.; Trachtenberg, J.; Lawrentschuk, N. Focal therapy in prostate cancer: modalities, findings and future considerations. *Nat. Rev. Urol.* **2010**, *7*, 562−571.
(72) Chen, D. Q.; Wang, C.; Nie, X.; Li, S. M.; Li, R. M.; Guan, M. R.; Liu, Z.; Chen, C. Y.; Wang, C. R.; Wan, L. J. Photoacoustic imaging guided near-infrared photothermal therapy using highly water-dispersible single-walled carbon nanohorns as theranostic agents. *Adv. Funct. Mater.* **2014**, *24*, 6621−6628.
(73) Han, K.; Wang, S. B.; Lei, Q.; Zhu, J. Y.; Zhang, X. Z. Ratiometric biosensor for aggregation-induced emission-guided precise photodynamic therapy. *ACS Nano* **2015**, *9*, 10268−10277.
(74) Shi, P.; Liu, Z.; Dong, K.; Ju, E. G.; Ren, J. S.; Du, Y. D.; Li, Z. Q.; Qu, X. G. A smart sense-act-treat system: combining a ratiometric pH sensor with a near infrared therapeutic gold nanocage. *Adv. Mater.* **2014**, *26*, 6635−6641.
(75) Myochin, T.; Kiyose, K.; Hanaoka, K.; Kojima, H.; Terai, T.; Nagano, T. Rational design of ratiometric near-infrared fluorescent pH probes with various pKa values, based on aminocyanine. *J. Am. Chem. Soc.* **2011**, *133*, 3401−3409.
(76) Tsai, Y. T.; Zhou, J.; Weng, H.; Shen, J. H.; Tang, L. P.; Hu, W. J. Real-time noninvasive monitoring of *in vivo* inflammatory responses using a pH ratiometric fluorescence imaging probe. *Adv. Healthcare Mater.* **2014**, *3*, 221−229.
(77) Albers, A. E.; Okreglak, V. S.; Chang, C. J. A FRET-based approach to ratiometric fluorescence detection of hydrogen peroxide. *J. Am. Chem. Soc.* **2006**, *128*, 9640−9641.
(78) Li, J.; Tian, C. C.; Yuan, Y.; Yang, Z.; Yin, C.; Jiang, R. C.; Song, W. L.; Li, X.; Lu, X. M.; Zhang, L.; Fan, Q. L.; Huang, W. A water-soluble conjugated polymer with pendant disulfide linkages to PEG chains: a highly efficient ratiometric probe with solubility-induced fluorescence conversion for thiol detection. *Macromolecules* **2015**, *48*, 1017−1025.
(79) Li, K.; Liu, B. Polymer-encapsulated organic nanoparticles for fluorescence and photoacoustic imaging. *Chem. Soc. Rev.* **2014**, *43*, 6570−6597.
(80) Feng, L.; Zhu, C.; Yuan, H.; Liu, L.; Lv, F.; Wang, S. Conjugated polymer nanoparticles: preparation, properties, functionalization and biological applications. *Chem. Soc. Rev.* **2013**, *42*, 6620−6633.
(81) Xu, L. G.; Cheng, L.; Wang, C.; Peng, R.; Liu, Z. Conjugated polymers for photothermal therapy of cancer. *Polym. Chem.* **2014**, *5*, 1573−1580.
(82) Peng, H. S.; Chiu, D. T. Soft fluorescent nanomaterials for biological and biomedical imaging. *Chem. Soc. Rev.* **2015**, *44*, 4699−4722.
(83) Yuan, Y.; Liu, J.; Liu, B. Conjugated-polyelectrolyte-based polyprodrug: targeted and image-guided photodynamic and chemotherapy with on-demand drug release upon irradiation with a single light source. *Angew. Chem., Int. Ed.* **2014**, *53*, 7163−7168.
(84) He, R.; Hu, M.; Xu, T.; Li, C.; Wu, C.; Guo, X.; Zhao, Y. Conjugated copolymer-photosensitizer molecular hybrids with broad-band visible light absorption for efficient light-harvesting and enhanced singlet oxygen generation. *J. Mater. Chem. C* **2015**, *3*, 973−976.
(85) Geng, J. L.; Sun, C. Y.; Liu, J.; Liao, L. D.; Yuan, Y. Y.; Thakor, N.; Wang, J.; Liu, B. Biocompatible conjugated polymer nanoparticles for efficient photothermal tumor therapy. *Small* **2015**, *11*, 1603−1610.
(86) Yuan, Y. Y.; Min, Y. Z.; Hu, Q. L.; Xing, B. G.; Liu, B. NIR photoregulated chemo-and photodynamic cancer therapy based on conjugated polyelectrolyte−drug conjugate encapsulated upconversion nanoparticles. *Nanoscale* **2014**, *6*, 11259−11272.
(87) Shi, S. Y.; He, Y. G.; Chen, W. W.; Liu, N.; Zhu, Y. Y.; Ding, Y. S.; Yin, J.; Wu, Z. Q. Enantiomer-selective polypeptide-b-poly(phenyl isocyanide) hybrid rod-rod copolymers: one-pot synthesis, self-assembly, and cell imaging. *Macromol. Rapid Commun.* **2015**, *36*, 1511−1520.
(88) Li, W.; He, Y. G.; Shi, S. Y.; Liu, N.; Zhu, Y. Y.; Ding, Y. S.; Yin, J.; Wu, Z. Q. Fabrication of multi-charges generable poly(phenyl isocyanide)-*block*- poly(3-hexylthiophene) rod-rod conjugated copolymer. *Polym. Chem.* **2015**, *6*, 2348−2355.
(89) Hong, Y.; Lam, J. W. Y.; Tang, B. Z. Aggregation-induced emission. *Chem. Soc. Rev.* **2011**, *40*, 5361−5388.
(90) Hong, Y.; Lam, J. W. Y.; Tang, B. Z. Aggregation-induced emission: phenomenon, mechanism and applications. *Chem. Commun.* **2009**, 4332−4353.
(91) Wang, M.; Zhang, G.; Zhang, D. Q.; Zhu, D. B.; Tang, B. Z. Fluorescent bio/chemosensors based on silole and tetraphenylethene luminogens with aggregation-induced emission feature. *J. Mater. Chem.* **2010**, *20*, 1858−1867.
(92) Tong, H.; Hong, Y. N.; Dong, Y. Q.; Häußler, M.; Li, Z.; Lam, J. W. Y.; Dong, Y. P.; Sung, H. H. Y.; Williams, I. D.; Tang, B. Z. Protein detection and quantitation by tetraphenylethene-based fluorescent probes with aggregation-induced emission characteristics. *J. Phys. Chem. B* **2007**, *111*, 11817−11823.

DOI: 10.1021/acs.macromol.7b00669
Macromolecules 2017, 50, 4114−4125

(93) Wu, W. B.; Feng, G. X.; Xu, S. D.; Liu, B. A photostable far-red/near-infrared conjugated polymer photosensitizer with aggregation-induced emission for image-guided cancer cell ablation. *Macromolecules* **2016**, *49*, 5017−5025.
(94) Yin, J.; Xu, L.; Han, X.; Zhou, L.; Li, C. L.; Wu, Z. Q. A facile synthetic route to stereoregular helical poly(phenyl isocyanide)s with defined pendants and controlled helicity. *Polym. Chem.* **2017**, *8*, 545−556.
(95) He, Y. G.; Shi, S. Y.; Liu, N.; Ding, Y. S.; Yin, J.; Wu, Z. Q. Tetraphenylethene-functionalized conjugated helical poly(phenyl isocyanide) with tunable light emission, assembly morphology, and specific applications. *Macromolecules* **2016**, *49*, 48−58.
(96) Xue, Y. X.; Chen, J. L.; Jiang, Z. Q.; Yu, Z. P.; Liu, N.; Yin, J.; Zhu, Y. Y.; Wu, Z. Q. Living polymerization of arylisocyanide initiated by the phenylethynyl palladium(II) complex. *Polym. Chem.* **2014**, *5*, 6435−6438.
(97) Chen, Y.; Zhang, Z. H.; Han, X.; Yin, J.; Wu, Z. Q. Oxidation and acid milieu-disintegratable nanovectors with rapid cell penetrating helical polymer chains for programmed drug release and synergistic chemo-photothermal therapy. *Macromolecules* **2016**, *49*, 7718−7727.
(98) Kitto, H. J.; Schwartz, E.; Nijemeisland, M.; Koepf, M.; Cornelissen, J. J. L. M.; Rowan, A. E.; Nolte, R. J. M. Post-modification of helical dipeptide polyisocyanides using the click reaction. *J. Mater. Chem.* **2008**, *18*, 5615−5624.
(99) Tang, H. Y.; Yin, L. C.; Kim, K. H.; Cheng, J. J. Helical poly(arginine) mimics with superior cell-penetrating and molecular transporting properties. *Chem. Sci.* **2013**, *4*, 3839−3844.

DOI: 10.1021/acs.macromol.7b00669
Macromolecules 2017, 50, 4114−4125